Wide Frequency Band Numerical Approaches for Multiple Scattering Problems by Disks

Xavier Antoine, Karim Ramdani, Bertrand Thierry

Wide frequency band numerical approaches for multiple scattering problems by disks

Xabier Antoine, Karim Ramdani, Bertrand Thierry
Institut Elie Cartan Nancy (Nancy-Université, CNRS, INRIA),
Université Henri Poincaré, BP 239, 54506,
Vandœuvre-lès-Nancy, France.
and
INRIA Nancy Grand-Est (Corida Team),
615 rue du Jardin Botanique,
54600 Villers-lès-Nancy, France.

ABSTRACT
Efficient, robust and accurate algorithms are proposed for solving the multiple scattering problem by M circular obstacles for the whole spectrum of frequency. The representation of the solution is based on an integral equation formulation next solved by using Fourier basis. Numerical examples are provided to show that the approaches are efficient.

Keywords: Multiple scattering; circular cylinders; wide frequency band; fast and accurate algorithms; preconditioning

1 INTRODUCTION

Let us consider M smooth, bounded and disjoint scatterers Ω_p^-, $p = 1, ..., M$, placed in $\mathbb{R}^2$. We denote by Γ_p the boundary of each single object Ω_p^-. The global scatterer Ω^- is defined as the union of the M obstacles: $\Omega^- = \cup_{p=1}^M \Omega_p^-$, and $\Gamma = \cup_{p=1}^M \Gamma_p$ is its boundary. The exterior domain of propagation is denoted by $\Omega^+ = \mathbb{R}^2 \setminus \overline{\Omega^-}$ and is assumed to be homogeneous and isotropic. Through out the paper, we assume that the scatterers are sound-soft (Dirichlet boundary condition), but other situations can be handled by slightly adapting our approach (e.g. sound-hard scatterers, impedance boundary condition, penetrable scatterers). Consider that an incident time-harmonic plane wave $u^{inc}(\mathbf{x}) = e^{ik\boldsymbol{\beta}\cdot\mathbf{x}}$ illuminates Ω^-, with an incidence direction $\boldsymbol{\beta} = (\cos(\beta), \sin(\beta))$ and a time dependence of the form $e^{-i\omega t}$, ω being the wave pulsation and k the related wavenumber. Then, the multiple scattering problem of u^{inc} by Ω^- amounts to

finding the scattered wavefield u solution to the boundary value problem

$$\begin{cases} (\Delta + k^2)u = 0 & (\Omega^+) \\ u = -u^{inc} & (\Gamma) \\ \lim\limits_{|\mathbf{x}|\to+\infty} |\mathbf{x}|^{1/2} \left(\nabla u \cdot \dfrac{\mathbf{x}}{|\mathbf{x}|} - iku \right) = 0 \end{cases} \tag{1.1}$$

The Laplace operator is $\Delta = \partial^2_{x_1} + \partial^2_{x_2}$ for a point $\mathbf{x} = (x_1, x_2) \in \mathbb{R}^2$ and $(\Delta + k^2)$ is the Helmholtz operator. The nabla operator ∇ is the usual gradient operator and $|\mathbf{x}| = \sqrt{\mathbf{x} \cdot \mathbf{x}}$ is the length of vector $\mathbf{x}$, denoting by $\mathbf{x} \cdot \mathbf{y}$ the inner product of two vectors $\mathbf{x}$ and $\mathbf{y}$ of $\mathbb{R}^2$. Finally, the last equation of system (1.1) is the so-called Sommerfeld's radiation condition at infinity and ensures the uniqueness of the solution u.

Multiple scattering problems have many applications. In particular, in the case of spheres, important applications are related to remote sensing [1], ultrasound interaction in tissue for cancer detection [2], photonics and phononics modelling [3, 4], near-field optical applications involving dielectric microspheres for electromagnetic photonic jets [5, 6] and confining 3D structures [7], plasmonic resonance from metallic nanoparticules [8, 9, 10], scattering by dielectric microstructured medium [11]... For these reasons, the development of an efficient numerical method for solving multiple scattering problems for M spheres and for a wide range of frequency is of upmost importance.

Concerning the numerical techniques, many papers are already available but essentially for low-frequencies (see e.g. [4, 12]). Medium/high frequency [13, 14, 15] is much less studied since it leads to very specific difficult numerical problems related to the strong coupling effects between scatterers and to the highly non definite character of the resulting complex linear system. Therefore, usual low-frequency numerical methods break down when they are applied to these configurations. We propose here to investigate in the case of circular cylinders some efficient numerical solutions for the wide frequency band. The plan of the paper is the following. In the second Section, we propose to formulate the problem under the form of an integral equation. Section 3 provides a Fourier spectral approach for approximating the solution of this equation. Sections 4 and 5 propose some robust and efficient numerical methods respectively for the low- and medium/high-frequency range with numerical examples. Finally, Section 6 gives a conclusion.

2 INTREGRAL EQUATION FORMULATIONS

To solve the multiple scattering problem (1.1), a possible approach is to consider an integral equation formulation. Other possible solutions are based on volumetric formulations using for example a PDE-based representation solved through a finite element method. However, this last solution can be computationally expensive in the case where the single scatterers are far from each other since it results in a large domain of computation or when the wavenumber is

high. With regards to integral equation formulations, an infinite number of representations are at hand when solving scattering by closed surface obstacles. We refer to [13] for a complete presentation of integral equations in the background of multiple scattering. Each integral representation has its own advantages and drawbacks from the point of view of mathematical (well-posedness, problems related to spurious resonances) and numerical (first-kind vs second-kind integral equations, conditioning problems) properties. Here, we choose to focus only on one integral equation for two reasons:

- first, the mathematical description of other possible integral formulations can be found in [13]. Furthermore, the developments in sections 2 and 3 can be adapted quite directly to general integral representations.
- second, from the numerical point of view, it appears that after preconditioning the two other classical integral equations MFIE (Magnetic Field Integral Equation) and CFIE (Combined Field Integral Equation) with a preconditioner built on the self-interaction scattering (see preconditioner 1 in Section 5), the integral equations reduce exactly to the same linear system. Of course, this is due to the particular geometry considered here (disks).

For these reasons, only the single-layer integral representation, also known as the Electric Field Integral Equation (EFIE), is studied. Let us recall some well-known facts about it (for more details, see for instance [16, 17]). The EFIE uses the following representation of the scattered field u

$$\forall \mathbf{x} \in \Omega^+, \qquad u(\mathbf{x}) = \mathcal{L}\rho(\mathbf{x}) = \int_\Gamma G(\mathbf{x},\mathbf{y})\rho(\mathbf{y})\, \mathrm{d}\Gamma(\mathbf{y}). \tag{2.1}$$

The single-layer operator $\mathcal{L}$ acts from $H^{-1/2}(\Gamma)$ onto $H^1_{loc}(\Omega^+) \cap H^1(\Omega^-)$ and the Green function $G(\mathbf{x},\mathbf{y})$ is

$$\forall (\mathbf{x},\mathbf{y}) \in \mathbb{R}^2 \times \mathbb{R}^2,\ \mathbf{x} \neq \mathbf{y},\ G(\mathbf{x},\mathbf{y}) = \frac{i}{4} H_0^{(1)}(k|\mathbf{x}-\mathbf{y}|),$$

where the function $H_0^{(1)}$ is the first-kind Hankel function of order zero. Based on (2.1), the density ρ becomes the new unknown of the scattering problem (1.1). A well-known property of the single-layer potential is that $\mathcal{L}\rho$ satisfies both the Sommerfeld's radiation condition and the Helmholtz equation in $\Omega^+ \cup \Omega^-$. Therefore, to solve the scattering problem (1.1), $\mathcal{L}\rho$ only needs to satisfy the Dirichlet boundary condition on Γ which requires taking the trace of $\mathcal{L}\rho$ on Γ. Before giving the result, let us introduce the set $F_D(\Omega^-)$ of Dirichlet irregular frequencies k for which the interior boundary value problem

$$\begin{cases} \Delta v + k^2 v = 0 & (\Omega^-) \\ v = 0 & (\Gamma) \end{cases}$$

admits non vanishing solutions. Clearly, $F_D(\Omega^-)$ is nothing but the union of the sets of Dirichlet irregular frequencies corresponding to each scatterer. Then, we have the following result.

Theorem 2.1. *If $k \notin F_D(\Omega^-)$, then $u = \mathcal{L}\rho$ solves the scattering problem if and only if ρ is the solution to the EFIE*

$$L\rho = -u^{inc}|_\Gamma, \qquad \text{in } H^{1/2}(\Gamma), \tag{2.2}$$

where the operator L is the single-layer boundary integral operator defined by

$$\forall \mathbf{x} \in \Gamma, \quad L\rho(\mathbf{x}) = \int_\Gamma G(\mathbf{x}, \mathbf{y})\rho(\mathbf{y})\, \mathrm{d}\Gamma(\mathbf{y}).$$

Moreover, the density ρ has a physical interpretation since it is given by the relation

$$\rho = (-\partial_{\mathbf{n}} u - \partial_{\mathbf{n}} u^{inc})_{|\Gamma}, \tag{2.3}$$

where $\mathbf{n}$ is the outward unit normal of Ω^-.

If $k \in F_D(\Omega^-)$, the EFIE is no more uniquely solvable. Indeed, any solution ρ^0 of the EFIE can be written as $\rho^0 = \rho + \rho^*$, where ρ is given by (2.3) and $\rho^* \in \mathrm{Ker}(L)$ is a spurious surface density. One can easily check that $\mathrm{Ker}(L) \subset \mathrm{Ker}(\mathcal{L})$, which implies that: $\mathcal{L}\rho^0 = \mathcal{L}(\rho + \rho^*) = \mathcal{L}\rho$. This means that the quantity $\mathcal{L}\rho^0$, obtained with an arbitrary solution ρ^0 of the EFIE, still defines the solution of the scattering problem (whose solution is of course unique). The spurious term $\mathcal{L}\rho^*$ is said to be "non radiating" and then should *a priori* not pollute for example the computation of the far-field pattern. However, the loss of uniqueness remains a problem and most particularly from the numerical point of view since the resulting linear system approximating the EFIE can be singular. This property is penalizing for the numerical simulations when one wants to compute a whole range of frequency, most particularly for large wavenumbers. In Section 5, we provide a modified formulation including preconditioning which avoids this problem.

3 A FOURIER SPECTRAL APPROACHI FOR CIRCULAR SCATTERERS

Let us now come to the numerical solution of the EFIE (2.2). A classical way to solve the problem is to use a boundary element method. While the method is very flexible concerning the shape of the scatterers, it leads to the solution to a large scale full linear system, most particularly for high frequency (when the wavenumber k is large compared to the characteristic size of each obstacle Ω_p^-) or/and when the number of obstacles is large: $M \gg 1$. We propose here to develop a spectral approach when the scatterers are circular cylinders. In this situation, we can use Fourier basis functions associated with each obstacle.

The first step consists in writing a weak formulation of (2.2) in $L^2(\Gamma)$. Note that this is possible since by classical regularity arguments, the unknown density $\rho \in H^{-1/2}(\Gamma)$ is in fact infinitely differentiable function. Multiplying Eq. (2.2) by a test-function $\Phi \in L^2(\Gamma)$ yields

$$\begin{cases} \text{Find } \rho \in L^2(\Gamma) \text{ such that} \\ \forall \Phi \in L^2(\Gamma), \ \ \langle L\rho, \Phi \rangle_{L^2(\Gamma)} = \left\langle -u^{inc}, \Phi \right\rangle_{L^2(\Gamma)}. \end{cases} \tag{3.1}$$

The brackets $\langle \cdot\,,\, \cdot \rangle$ denotes the usual hermitian scalar product on $L^2(\Gamma)$

$$\forall (f,g) \in L^2(\Gamma) \times L^2(\Gamma), \quad \langle f, g \rangle_{L^2(\Gamma)} = \int_\Gamma f \overline{g} \, \mathrm{d}\Gamma.$$

If $(\Psi_m)_{m\in\mathbb{Z}}$ is an orthonormal basis of $L^2(\Gamma)$, the weak formulation can be written equivalently as

$$\begin{cases} \text{Find } \rho \in L^2(\Gamma) \text{ such that} \\ \forall m \in \mathbb{Z}, \;\; \langle L\rho, \Psi_m \rangle_{L^2(\Gamma)} = \left\langle -u^{inc}|_\Gamma, \Psi_m \right\rangle_{L^2(\Gamma)}. \end{cases} \tag{3.2}$$

Since we are considering circular boundaries Γ_p, a suitable choice of orthonormal basis is the Fourier basis. More precisely, the spectral approximation that we propose is built by using M Fourier basis, one per scatterer, that are then gathered to obtain an orthonormal basis of $L^2(\Gamma_1) \times L^2(\Gamma_2) \times \ldots \times L^2(\Gamma_M)$. Each obstacle Ω_p^-, $p = 1, \ldots, M$, is a disk centered at $\mathbf{O}_p$ with radius a_p. A point $\mathbf{x} \in \mathbb{R}^2$ is described by its local polar coordinates associated with the scatterer Ω_p^-

$$\mathbf{r}_p(\mathbf{x}) = \mathbf{O}_p\mathbf{x}, \qquad r_p(\mathbf{x}) = |\mathbf{r}_p(\mathbf{x})|, \qquad \theta_p(\mathbf{x}) = \mathrm{Angle}(\overrightarrow{Ox_1}, \mathbf{r}_p(\mathbf{x})).$$

We also need the vectors $\mathbf{b}_p$ pointing from the origin $\mathbf{O}$ to the center $\mathbf{O}_p$

$$\mathbf{b}_p = \mathbf{O}\mathbf{O}_p, \qquad b_p = |\mathbf{b}_p|, \qquad \alpha_p = \mathrm{Angle}(\overrightarrow{Ox_1}, \mathbf{b}_p),$$

and the vectors $\mathbf{b}_{pq}$ between the centers $\mathbf{O}_q$ and $\mathbf{O}_p$ of two separate disks Ω_q^- and Ω_p^-

$$\mathbf{b}_{pq} = \mathbf{O}_q\mathbf{O}_p, \qquad b_{pq} = |\mathbf{b}_{pq}|, \qquad \alpha_{pq} = \mathrm{Angle}(\overrightarrow{Ox_1}, \mathbf{b}_{pq}), \qquad 1 \le p \ne q \le M.$$

For each scatterer Ω_p^-, $p = 1, \ldots, M$, we introduce the Fourier basis functions $(\varphi_m^p)_{m\in\mathbb{Z}}$, defined by

$$\forall m \in \mathbb{Z}, \quad \forall \mathbf{x} \in \Gamma_p, \quad \varphi_m^p(\mathbf{x}) = \frac{e^{im\theta_p(\mathbf{x})}}{\sqrt{2\pi a_p}}.$$

This family forms an orthonormal basis of $L^2(\Gamma_p)$. We now gather these M families by introducing the functions $(\Phi_m^p)_{m\in\mathbb{Z},p=1,\ldots,M}$ defined by

$$\forall p, q \in \{1, \ldots, M\}, \forall m \in \mathbb{Z}, \qquad \Phi_m^p|_{\Gamma_q} = \begin{cases} \varphi_m^p, & \text{if } p = q, \\ 0, & \text{otherwise.} \end{cases} \tag{3.3}$$

Finally, $\mathcal{B} = (\Phi_m^p)_{m\in\mathbb{Z},p=1,\ldots,M}$ is an orthonormal basis of $L^2(\Gamma)$. For the sake of clarity, it is referred to as the Fourier basis.

The next step is to express the weak formulation (3.2) in $\mathcal{B}$. To achieve this, the density ρ is decomposed as

$$\rho = \sum_{p=1}^{M} \sum_{m\in\mathbb{Z}} \rho_m^p \Phi_m^p. \tag{3.4}$$

The weak formulation is then

$$\begin{cases} \text{Find the Fourier coefficients } (\rho_n^q)_{q=1,\dots,M,n\in\mathbb{Z}} \text{ such that} \\ \forall p \in \{1,\dots,M\}, \forall m \in \mathbb{Z},\ \displaystyle\sum_{q=1}^{M}\sum_{n\in\mathbb{Z}} \mathbb{L}_{m,n}^{p,q}\rho_n^q = f_m^p, \end{cases} \tag{3.5}$$

where the coefficients $\mathbb{L}_{m,n}^{p,q}$ and f_m^p are given by

$$\mathbb{L}_{m,n}^{p,q} = \langle L\Phi_n^q, \Phi_m^p\rangle_{L^2(\Gamma)}, \qquad f_m^p = \left\langle -u^{inc}|_\Gamma, \Phi_m^p \right\rangle_{L^2(\Gamma)}.$$

The coefficients f_m^p of the incident wave can be obtained analytically through a short calculation [12, p. 125]

$$f_m^p = -\sqrt{2\pi a_p}\, e^{im(\pi/2-\beta)} J_m(ka_p), \qquad \forall p = 1,\dots,M, \forall m \in \mathbb{Z}.$$

Concerning the coefficients $\mathbb{L}_{m,n}^{p,q}$ of the infinite system (3.5), we first consider the case of the diagonal blocks ($p = q$) and use the following result (see [18]).

Theorem 3.1. *For $p = 1,\dots,M$ and $m,n \in \mathbb{Z}$, we have*

$$\mathbb{L}_{m,n}^{p,p} = \delta_{mn}\frac{i\pi a_p}{2} J_m(ka_p)H_m^{(1)}(ka_p),$$

where δ_{mn} denotes the Krönecker symbol and the functions J_m and $H_m^{(1)}$ are respectively the Bessel and first-kind Hankel functions of order m.

For the off-diagonal blocks corresponding to $p \neq q$, we have to decompose the Green's function $G(\mathbf{x},\mathbf{y})$ in the basis $\mathcal{B}$. This can be achieved thanks to the so-called "two-centre expansion" [12, Theorem 2.14].

Theorem 3.2 (Two-centre expansion)**.** *Let $p,q \in \mathbb{Z}$ such that $1 \le p \neq q \le M$. Then, for any points $\mathbf{x} \in \Gamma_p$ and $\mathbf{y} \in \Gamma_q$, the following two-centre expansion holds*

$$H_0^{(1)}(k\|\mathbf{x}-\mathbf{y}\|) = 2\pi\sqrt{a_p a_q}\sum_{n\in\mathbb{Z}}\sum_{m\in\mathbb{Z}} J_m(ka_p)S_{nm}(b_{pq})J_n(ka_q)\overline{\varphi_n^q(\mathbf{y})}\varphi_m^p(\mathbf{x}), \tag{3.6}$$

where the separation functions S_{nm} are defined by

$$S_{nm}(\mathbf{b}_{pq}) = H_{n-m}^{(1)}(kb_{pq})e^{i(n-m)\alpha_{pq}}, \qquad \forall m,n \in \mathbb{Z}.$$

Now we are able to compute all the coefficients $\mathbb{L}_{m,n}^{p,q}$.

Proposition 3.3. *For all $1 \le p,q \le M$, and for all m,n in $\mathbb{Z}$, we have*

$$\mathbb{L}_{m,n}^{p,q} = \begin{cases} \delta_{mn}\dfrac{i\pi a_p}{2} J_m(ka_p)H_m^{(1)}(ka_p), & \text{if } p = q, \\ \dfrac{i\pi\sqrt{a_p a_q}}{2} J_m(ka_p)S_{nm}(b_{pq})J_n(ka_q), & \text{otherwise.} \end{cases} \tag{3.7}$$

Proof. Let $1 \leq p, q \leq M$ be two scatterers indices and $m, n \in \mathbb{Z}$ two indices of the Fourier coefficients. For $p = q$, the expression of the coefficients $\mathbb{L}^{p,p}_{m,n}$ are given by Theorem 3.1. For $p \neq q$, the coefficients $\mathbb{L}^{p,q}_{m,n}$ read as

$$\mathbb{L}^{p,q}_{m,n} = \langle L\Phi^q_n, \Phi^p_m \rangle_{L^2(\Gamma)} = \int_\Gamma \int_\Gamma \frac{i}{4} H^{(1)}_0(k|\mathbf{x}-\mathbf{y}|)\Phi^q_n(\mathbf{y})\, \mathrm{d}\Gamma(\mathbf{y})\overline{\Phi^p_m(\mathbf{x})}\, \mathrm{d}\Gamma(\mathbf{x}). \tag{3.8}$$

Plugging the expressions of functions Φ^p_m and Φ^q_n in Eq. (3.8), the above integrals become integrals on Γ_p and Γ_q:

$$\mathbb{L}^{p,q}_{m,n} = \frac{i}{4} \int_{\Gamma_p} \int_{\Gamma_q} H^{(1)}_0(k|\mathbf{x}-\mathbf{y}|)\varphi^q_n(\mathbf{y})\overline{\varphi^p_m(\mathbf{x})}\, \mathrm{d}\Gamma_q(\mathbf{y})\mathrm{d}\Gamma_p(\mathbf{x}). \tag{3.9}$$

Since $\mathbf{x} \in \Gamma_p$ while $\mathbf{y} \in \Gamma_q$, our goal is now to split the two integrals to use the orthonormality property of functions $(\varphi^p_m)_{m\in\mathbb{Z},p=1,\dots,M}$ on $L^2(\Gamma_p)$ and $L^2(\Gamma_q)$ respectively. To achieve this, we use the two-centre expansion of Theorem 3.2. Using (3.6) in (3.9) gives

$$\mathbb{L}^{p,q}_{m,n} = \frac{i2\pi\sqrt{a_p a_q}}{4} \int_{\Gamma_p} \int_{\Gamma_q} \sum_{n_1\in\mathbb{Z}} \sum_{m_1\in\mathbb{Z}} J_{m_1}(ka_p) S_{n_1 m_1}(\mathbf{b}_{pq}) J_{n_1}(ka_q) \overline{\varphi^q_{n_1}(\mathbf{y})}\varphi^p_{m_1}(\mathbf{x}) \\ \varphi^q_n(\mathbf{y})\overline{\varphi^p_m(\mathbf{x})}\, \mathrm{d}\Gamma_q(\mathbf{y})\mathrm{d}\Gamma_p(\mathbf{x}).$$

The two integrals can be separated by inverting the integrals and sums

$$\mathbb{L}^{p,q}_{m,n} = \frac{i\pi\sqrt{a_p a_q}}{2} \sum_{n_1\in\mathbb{Z}} \sum_{m_1\in\mathbb{Z}} J_{m_1}(ka_p) S_{n_1 m_1}(\mathbf{b}_{pq}) J_{n_1}(ka_q) \int_{\Gamma_p} \varphi^p_{m_1}(\mathbf{x})\overline{\varphi^p_m(\mathbf{x})}\, \mathrm{d}\Gamma_p(\mathbf{x}) \\ \int_{\Gamma_q} \varphi^q_n(\mathbf{y})\overline{\varphi^q_{n_1}(\mathbf{y})}\, \mathrm{d}\Gamma_q(\mathbf{y}).$$

Finally, using the orthonormality of the basis functions leads to

$$\mathbb{L}^{p,q}_{m,n} = \frac{i\pi\sqrt{a_p a_q}}{2} J_m(ka_p) S_{nm}(\mathbf{b}_{pq}) J_n(ka_q),$$

ending hence the proof. □

In view of a numerical treatment, it is more convenient to write our problem (3.5) as an infinite matrix form

$$\widetilde{\mathbb{L}}\widetilde{\boldsymbol{\rho}} = \widetilde{\mathbf{f}}, \tag{3.10}$$

with the following block structure

$$\begin{pmatrix} \widetilde{\mathbb{L}}^{1,1} & \widetilde{\mathbb{L}}^{1,2} & \dots & \widetilde{\mathbb{L}}^{1,M} \\ \widetilde{\mathbb{L}}^{2,1} & \widetilde{\mathbb{L}}^{2,2} & \dots & \widetilde{\mathbb{L}}^{2,M} \\ \vdots & \vdots & \ddots & \vdots \\ \widetilde{\mathbb{L}}^{M,1} & \widetilde{\mathbb{L}}^{M,2} & \dots & \widetilde{\mathbb{L}}^{M,M} \end{pmatrix} \begin{pmatrix} \widetilde{\boldsymbol{\rho}}^1 \\ \widetilde{\boldsymbol{\rho}}^2 \\ \vdots \\ \widetilde{\boldsymbol{\rho}}^M \end{pmatrix} = \begin{pmatrix} \widetilde{\mathbf{f}}^1 \\ \widetilde{\mathbf{f}}^2 \\ \vdots \\ \widetilde{\mathbf{f}}^M \end{pmatrix}, \tag{3.11}$$

where

- The infinite blocks $\widetilde{\mathbb{L}}^{p,q} = (\mathbb{L}^{p,q}_{m,n})_{m,n\in\mathbb{Z}}$, for $1 \le p, q \le M$ are given by

$$\widetilde{\mathbb{L}}^{p,q} = \begin{cases} \dfrac{i\pi a_p}{2}\widetilde{\mathbb{J}}^p\widetilde{\mathbb{H}}^p, & \text{if } p = q, \\ \dfrac{i\pi\sqrt{a_p a_q}}{2}\widetilde{\mathbb{J}}^p(\widetilde{\mathbb{S}}^{p,q})^T\widetilde{\mathbb{J}}^q, & \text{otherwise,} \end{cases} \tag{3.12}$$

  in which the diagonal operators $\widetilde{\mathbb{J}}^p$ and $\widetilde{\mathbb{H}}^p$ have the coefficients $J_m(ka_p)$ and $H^{(1)}_m(ka_p)$ respectively. The infinite matrix $(\widetilde{\mathbb{S}}^{p,q})^T$ is the transposed matrix of $\widetilde{\mathbb{S}}^{p,q}$ defined by

$$\widetilde{\mathbb{S}} = (\mathbb{S}^{p,q}_{m,n})_{m,n\in\mathbb{Z}}, \qquad \widetilde{\mathbb{S}}^{p,q}_{m,n} = S_{mn}(\mathbf{b}_{pq}). \tag{3.13}$$

- The unknown infinite vector $\widetilde{\boldsymbol{\rho}}^p = (\rho^p_m)_{m\in\mathbb{Z}}$, for $p = 1, \dots, M$, contains the coefficients of the unknown ρ in the Fourier basis of $L^2(\Gamma_p)$.

- The right-hand side infinite vector $\widetilde{\mathbf{f}}^p = (f^p_m)_{m\in\mathbb{Z}}$, for $p = 1, \dots, M$, is the vector of Fourier coefficients of the trace of $-u^{inc}$ on Γ_p.

The diagonal blocks $\widetilde{\mathbb{L}}^{p,p}$ are connected to the self-interaction of the scatterer Ω^-_p whereas the off-diagonal blocks $\widetilde{\mathbb{L}}^{p,q}$, $1 \le p, q \le M$, $p \ne q$, represent the scattering coupling effect from the obstacle Ω^-_q onto Ω^-_p via the single-layer operator. Furthermore, the off-diagonal blocks are full while the diagonal blocks are diagonal.

Let us assume now that we have been able to compute the Fourier coefficients of ρ by solving Eq. (3.10). Then, it is possible to compute any quantity of physical interest like the scattered field at every point $\mathbf{x} \in \Omega^+$, its normal trace on Γ, and even the far-field pattern as it is shown in the proposition below [19].

Proposition 3.4. *For every point* $\mathbf{x}$ *in the propagation domain* Ω^+*, the scattered field* u *can be evaluated at* $\mathbf{x}$ *by the relation*

$$u(\mathbf{x}) = \sum_{p=1}^{M}\sum_{m\in\mathbb{Z}} \rho^p_m \frac{i\pi a_p}{2} J_m(ka_p) H^{(1)}_m(kr_p(\mathbf{x})) \frac{e^{im\theta_p(\mathbf{x})}}{\sqrt{2\pi a_p}}. \tag{3.14}$$

Furthermore, in the direction $\boldsymbol{\theta} = (\cos(\theta), \sin(\theta))$*,* $\theta \in [0, 2\pi]$*, we have*

$$u(\boldsymbol{\theta}|\mathbf{x}|) = \frac{e^{ik|\mathbf{x}|}}{|\mathbf{x}|^{1/2}} A(\theta) + \mathcal{O}\left(\frac{1}{|\mathbf{x}|}\right), \qquad \text{as } |\mathbf{x}| \to +\infty,$$

where the amplitude A *is given by*

$$A(\theta) = \frac{e^{i\pi/4}}{2\sqrt{k}} \sum_{p=1}^{M} \sqrt{a_p} e^{-ib_p k\cos(\theta-\alpha_p)} \left(\sum_{m\in\mathbb{Z}} e^{im(\theta-\frac{\pi}{2})} J_m(ka_p)\rho^p_m \right). \tag{3.15}$$

Proof. Let $\mathbf{x} \in \Omega^+$. By using the decomposition (3.4) of ρ in the expression of u (2.1), we get

$$u(\mathbf{x}) = \frac{i}{4} \sum_{p=1}^{M} \sum_{m \in \mathbb{Z}} \rho_m^p \int_\Gamma H_0^{(1)}(k|\mathbf{x}-\mathbf{y}|) \Phi_m^p(\mathbf{y}) \, \mathrm{d}\Gamma(\mathbf{y}).$$

Each integral can be reduced to Γ_p thanks to (3.3)

$$u(\mathbf{x}) = \frac{i}{4} \sum_{p=1}^{M} \sum_{m \in \mathbb{Z}} \frac{\rho_m^p}{\sqrt{2\pi a_p}} \int_{\Gamma_p} H_0^{(1)}(k|\mathbf{x}-\mathbf{y}|) e^{im\theta_p(\mathbf{y})} \, \mathrm{d}\Gamma(\mathbf{y}). \tag{3.16}$$

We observe now that $\mathbf{x} \in \Omega^+$ and $\mathbf{y} \in \Gamma_p$. As in the proof of Proposition 3.3, we decompose the Hankel's function in the Fourier basis thanks to Graff's addition theorem [12, Theorem 2.12]

$$H_0^{(1)}(k|\mathbf{x}-\mathbf{y}|) = \sum_{n \in \mathbb{Z}} J_n(ka_p) e^{-in\theta_p(\mathbf{y})} H_n^{(1)}(kr_p(\mathbf{x})) e^{in\theta_p(\mathbf{x})}. \tag{3.17}$$

Then, plugging (3.17) into (3.16) gives the sought relation (3.14).

Now, let us write $\mathbf{x} = \boldsymbol{\theta}\,|\mathbf{x}|$, with $\boldsymbol{\theta} = (\cos(\theta), \sin(\theta))$, $\theta \in [0, 2\pi]$. The expression of the far-field pattern (3.15) is then obtained by using both relation $r_p(\mathbf{x}) = |\mathbf{x}| - b_p \cos(\theta - \alpha_p) + \mathcal{O}\left(\frac{1}{|\mathbf{x}|}\right)$ and the asymptotic expansion of the Hankel's function $H_0^{(1)}(kr_p(\mathbf{x}))$ as $|\mathbf{x}|$ tends to infinity (see for instance (9.2.3) in [20]) in the expression of u (3.14). □

To conclude this section, let us analyze the connections between the method based on the integral representation and the Mie series (see for example [15]). Actually, in the Mie series approach, the scattered field u is sought as an infinite linear combination of cylindrical wave functions

$$u(\mathbf{x}) = \sum_{p=1}^{M} \sum_{m \in \mathbb{Z}} c_m^p H_m^{(1)}(kr_p(|\mathbf{x}|)) e^{im\theta_p(\mathbf{x})},$$

where the coefficients $(c_m^p)_{m \in \mathbb{Z}, p=1,\ldots,M}$ are unknown. Compared to (3.14), we have

$$\forall m \in \mathbb{Z}, \forall p, 1 \leq p \leq M, \qquad c_m^p = \frac{i}{2} \sqrt{\frac{\pi a_p}{2}} J_m(ka_p) \rho_m^p,$$

which means that the coefficients are the same up to a diagonal matrix multiplication. This can be generalized to the case of a linear combination between the single- and double-layer potentials. If we precondition the EFIE matrix $\widetilde{\mathbb{L}}$ by the self-interactions (see Section 5), then the two other classical formulations Magnetic Field Integral Equation (MFIE) and Combined Field Integral Equation (CFIE), which is well-posed for any wavenumber [13], are equivalent. This makes the resulting preconditioned formulation robust and free of spurious eigenfrequencies. We see in Section 5 that this must be done imperatively for medium/high frequency problems to get an improved convergence of the restarted GMRES.

4 NUMERICAL SOLUTION FOR THE LOW-FREQUENCY REGIME

Let us begin by considering first a low-frequency problem which means that $ka_p \ll 1$, for $1 \leq p \leq M$. The first problem that arises when solving the infinite system (3.10) is to adapt the spectral approximation parameters N_p for each obstacle. This leads to consider $2N_p + 1$ modes per Fourier series expansion since $-N_p \leq m \leq N_p$. Obviously, the truncation parameters $(N_p)_{p=1,\dots,M}$ can be chosen differently for each scatterer, depending on the radius a_p of each obstacle Ω_p^- as well as the frequency parameter k. If we truncate our series expansion at N_p by projecting the Fourier series solution on a finite dimensional space, then the associated linear sytem to solve is

$$\mathbb{L}\boldsymbol{\rho} = \mathbf{f}, \tag{4.1}$$

or

$$\begin{pmatrix} \mathbb{L}^{1,1} & \mathbb{L}^{1,2} & \dots & \mathbb{L}^{1,M} \\ \mathbb{L}^{2,1} & \mathbb{L}^{2,2} & \dots & \mathbb{L}^{2,M} \\ \vdots & \vdots & \ddots & \vdots \\ \mathbb{L}^{M,1} & \mathbb{L}^{M,2} & \dots & \mathbb{L}^{M,M} \end{pmatrix} \begin{pmatrix} \boldsymbol{\rho}^1 \\ \boldsymbol{\rho}^2 \\ \vdots \\ \boldsymbol{\rho}^M \end{pmatrix} = \begin{pmatrix} \mathbf{f}^1 \\ \mathbf{f}^2 \\ \vdots \\ \mathbf{f}^M \end{pmatrix},$$

where

- the block $\mathbb{L}^{p,q} = (\mathbb{L}^{p,q}_{m,n})_{-N_p \leq m \leq N_p, -N_q \leq n \leq N_q}$ is the $(2N_p+1) \times (2N_q+1)$ matrix, with coefficients $\mathbb{L}^{p,q}_{m,n}$ given by (3.7). As for the infinite dimensional system, these blocks can be written in a compact matrix form

$$\mathbb{L}^{p,q} = \begin{cases} \dfrac{i\pi a_p}{2} \mathbb{J}^p \mathbb{H}^p, & \text{if } p = q, \\ \dfrac{i\pi\sqrt{a_p a_q}}{2} \mathbb{J}^p (\mathbb{S}^{p,q})^T \mathbb{J}^q, & \text{otherwise,} \end{cases}$$

  where the notation without the tilde denotes the finite dimensional approximation version of system (3.10).

- $\boldsymbol{\rho}^p = (\rho^p_m)_{-N_p \leq m \leq N_p}$ is a finite vector containing $2N_p + 1$ coefficients which are approximations of those of ρ in the Fourier basis for Ω_p^-.

- $\mathbf{f}^p = (f^p_m)_{-N_p \leq m \leq N_p}$ is the finite vector containing the first $2N_p + 1$ coefficients of the incident wave in the Fourier basis corresponding to Ω_p^-.

As we assumed to be in a low frequency regime (ka_p are all small), one can expect that only a few modes can be kept to get an accurate solution. To confirm this, we consider the scattering configuration reported on Figure 1(a) which consists in taking $M = 200$ unit circular cylinders randomly distributed in the box $[-25; 25]^2$ for a frequency $k = 0.1$ (so that $ka_p = 0.1$). In the far-field, only the propagative modes plays a role and can be observed in the Radar Cross Section calculation: $\mathrm{RCS}(\theta) = 10 \log_{10}(2\pi |A(\theta)|^2)$ (dB). For our configuration, let us consider a reference calculation RCS^{ref} with $N_p = 15$

and let us analyze the error $\Delta\text{RCS} = \|\text{RCS}^{ref} - \text{RCS}^{N_p}\|_\infty$ for the L^∞ norm : $\|f(\theta)\|_\infty = \max_{0\leq\theta\leq 2\pi} |f(\theta)|$. The results are reported on Figure 1(b) showing the decay of the error according to N_p ("Direct solution"). This suggests that an accurate computation of the RCS can be obtained for $N_p = 2$, leading to an error of about 10^{-3} dB. Next, let us make a few comments on multiple scattering effects in this low-frequency regime. We report on Figure 1(c) the modulus of each Fourier mode (ρ_m^p) for $-N_p \leq m \leq N_p = 15$, $1 \leq p \leq M$ (referred to as "multiple scattering"). Here we only show the modes corresponding to a few scatterers and not the whole set of disks (the linear system is solved by a direct Gauss elimination solver). For comparison, we also draw the absolute values of the Fourier modes for a single disk and report it for each obstacle. We can see that the propagative modes for the multiple scattering problem are always smaller in amplitude than the corresponding ones for the single scattering problem. This expresses the fact that the multiple scattering medium behaves like a dissipative medium, as predicted by the Lax-Foldy theory [12]. Furthermore, we also observe that some high-order evanescent modes are excited by multiple scattering effects and are more important than for the single scattering problem. In the case of a near-field calculation, these should be included for an accurate computation. On this example, we can finally remark that some obstacles are invisible in the sense that their Fourier coefficients are very small. To conclude the low frequency analysis, we propose to take a look at the numerical solution of the truncated linear system. To this end, we report on Figure 1(d) ($k = 0.1$) the CPU time required for solving the system when M increases (the filling box is $[-65; 65]^2$) by using a direct Gauss elimination solver or the GMRES iterative Krylov solver [21] with restart parameter 50 and a tolerance $\varepsilon = 10^{-4}$ (this is denoted by GMRES(50, 10^{-4})). This last choice is sufficient when considering $N_p = 2$ as it can be observed on Figure 1(b) for RCS computations. Higher accuracy would impose a smaller value of ε. Choosing the Krylov solver finally reduces the computational time to 50% of the direct solution for $N_p = 2$. This is most particularly interesting for dense media where M becomes very large. It is to notice that further improvement would include preconditioning techniques.

5 NUMERICAL SOLUTION FOR THE MEDIUM AND HIGH-FREQUENCY REGIMES

The previous numerical solution was adapted to the low-frequency regime. However, the direct solution cannot be applied directly to the high frequency regime (ka_p very large) since the computational cost grows rapidly. Indeed, roughly speaking, a higher frequency requires more than $N_p = 2$ modes. In fact, it can be shown that, adapting the developments in [15], we must retain a number of modes equal to

$$N_p = \left[ka_p + \left(\frac{1}{2\sqrt{2}} \ln(2\sqrt{2}\pi k a_p \varepsilon^{-1}) \right)^{\frac{2}{3}} (ka_p)^{1/3} + 1 \right], \tag{5.1}$$

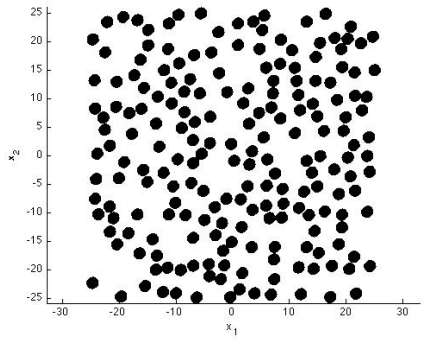

(a) Scattering configuration

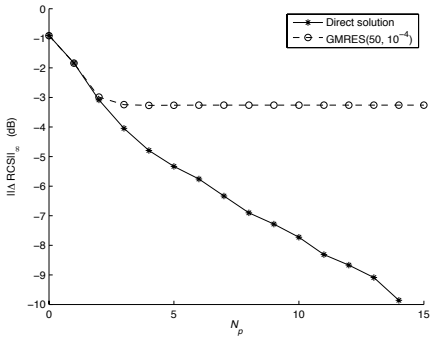

(b) Accuracy of the RCS approximation

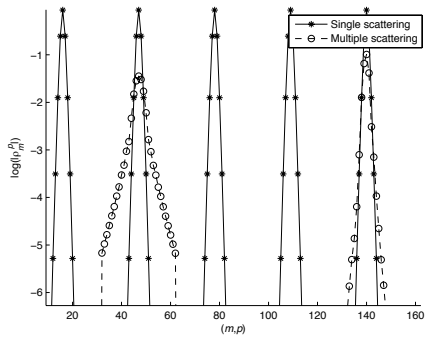

(c) Modes representation

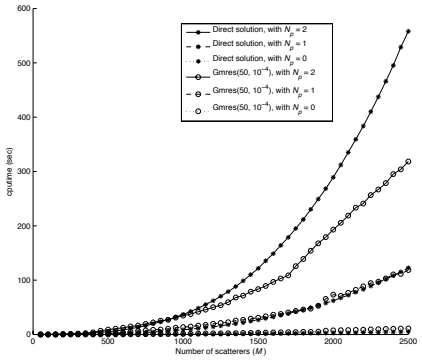

(d) Numerical solution of the linear system

Figure 1: Numerical solution for low-frequencies

where ε is the desired error bound on the Fourier coefficients (which is also the GMRES error parameter next). Remark that this formula is adapted to the size of each scatterer. Then, the direct solution needs a memory storage $\mathcal{O}\left([ka]^2M^2\right)$ and the direct solution of the linear system is done with $\mathcal{O}\left([ka]^3M^3\right)$ operations, if we assume that $a_p \approx a$, for $1 \leq p \leq M$. In fact, both costs can be reduced if we make the following remark. Let us introduce $N = \sum_{p=1}^{M}(2N_p+1)$. At first view, the matrix $\mathbb{L}$ is full. However, it appears that $\mathbb{L}$ has a sparse structure by blocks. Indeed, its diagonal blocks $\mathbb{L}^{p,p}$ are obtained through the products of two diagonal matrices $\mathbb{J}^p \in \mathbb{C}^{2N_p+1,2N_p+1}$ and $\mathbb{H}^p \in \mathbb{C}^{2N_p+1,2N_p+1}$ (which are trivially sparse). Furthermore, the off-diagonal blocks $\mathbb{L}^{p,q}$ can be written through the products of two diagonal matrices $\mathbb{J}^p$ and $\mathbb{J}^q$, and the matrix $(\mathbb{S}^{p,q})^T \in \mathbb{C}^{2N_p+1,2N_q+1}$ which is Toeplitz since its coefficients

$$\mathbb{S}^{p,q}_{m,n} = H^{(1)}_{m-n}(kb_{pq})e^{i(m-n)\alpha_{pq}},$$

only depends on $(m-n)$. As a consequence, a sparse storage of the matrix $(\mathbb{S}^{p,q})^T$ is given by the root vector γ^{pq} (built with the first row and column of the matrix $(\mathbb{S}^{p,q})^T$)

$$\gamma^{pq} = (S^{pq}_{Nq,-N_p}, \ldots, S^{pq}_{-Nq+1,-N_p}, S^{pq}_{-Nq,-N_p}, \ldots, S^{pq}_{-Nq,N_p})^T.$$

Finally, counting the total number of coefficients to store for the whole matrix gives $2N(2M-1)$ coefficients compared with the initial N^2 cost for the full storage. We report on Figures 2(a) ($ka_p = 200$, $1 \leq p \leq M$) and 2(b)($M = 100$, $a_p = 1$, $1 \leq p \leq M$) the number of stored coefficients for the full and compressed storages with respect to M and k. Here, we have considered that $\varepsilon = 10^{-4}$ in the GMRES and Equation (5.1). We can see that, in both cases, the sparse storage allows to consider much more complex situations for large wave numbers k and many obstacles M. The counterpart of this compressed storage is that we cannot use a direct solver for the linear system. This is a further reason for considering an iterative solution which is also consistent with the low-frequency study. Here, we consider the restarted GMRES$(50, 10^{-4})$ solution with tolerance ε $(= 10^{-4})$, this last parameter fixing N_p given by (5.1). The global cost of the GMRES is linked to the cost of one Matrix-Vector Product (MVP) times the number of iterations n^{iter}. Each MVP can be computed in a fast and accurate way by using an FFT-based algorithm for the MVP related to the Toeplitz parts of $\mathbb{L}$. Then, the global cost of a MVP is $\mathcal{O}(60(M-1)^2 ka \log_2(4ka))$ which must be compared with $\mathcal{O}(4(M-1)^2(ka)^2)$ for the direct MVP. Concerning the acceleration of the convergence, we propose two preconditioners. The first one consists in preconditioning the system by its diagonal part which corresponds to incorporating the single scattering effects. This preconditioner is denoted by "P1" in the sequel. Doing this, we have a linear system with a matrix $\widehat{\mathbb{L}}$ of the form: $\widehat{\mathbb{L}} = \mathbb{I} + \widehat{\mathbb{F}}$, where $\mathbb{I}$ is the identity matrix and $\widehat{\mathbb{F}}$ contains the off-diagonal blocks of $\widehat{\mathbb{L}}$. Then, we propose a second preconditioner (called "P2" in the following) which is built by two successive approximations. The first one consists in approximating $\widehat{\mathbb{L}}^{-1}$ by the two first terms of its Neumann

series: $\widehat{\mathbb{L}}^{-1} \sim \mathbb{I} - \widehat{\mathbb{F}} = \mathbb{P}$. At this point, the preconditioning matrix remains "full" because of $\widehat{\mathbb{F}}$. To sparsify it, we only retain the blocks corresponding to the closest interactions as a second approximation, leading hence to our sparse explicit preconditioner. We refer to [15] where a similar strategy is described with more details. We report the CPU time needed to build the matrix and solve the linear system as a function of M on Figure 2(c) and of k on Figure 2(d), with the different strategies. In Figures 2(c), we fix $ka = 200$ and increase the number M of obstacles in the computational box $[-25; 25]^2$, with GMRES$(50, 10^{-4})$. The minimal distance between scatterers is 0.5. In Figure 2(d), we compute for $M = 50$ obstacles the CPU time for ka growing, with a minimal distance 0.5 between the disks contained in the box $[-15; 15]^2$ for GMRES$(50, 10^{-4})$. We can observe a strong limitation of the direct approach compared with our fast algorithm. Concerning the GMRES solution, preconditioning is necessary, otherwise, the iterative method diverges. This is probably due to zeros of the Bessel functions. This can be corrected by the introduction of the preconditioner P1, and then P1 combined to P2 (it is worth noticing that using P1 or P2 for low frequencies yields a divergence of the iterative algorithm). The preconditioner P1-P2 can sometimes provide a convergence improvement when the scatterers are sufficiently far enough or for a regular lattice. When the situation is different, for example very close obstacles, then P1 seems to be more robust. This shows that building a preconditioner for this kind of problem is relatively an open question even if P1 already works well. This also confirms the remark at the end of Section 3 concerning the fact that preconditioning by P1 gives a well-posed and robust integral formulation for any frequency.

6 CONCLUSION

We have presented a formulation of the multiple scattering problem by circular cylinders based on integral equation representation. The method yields the numerical solution of a linear system. According to the frequency regime, different numerical strategies have been proposed for an efficient and convergent accurate computation. Further developments include penetrable scatterers, three-dimensional acoustic and electromagnetic scattering problems.

References

[1] K.H. Ding L. Tsang, J.A. Kong and C.O. Ao. *Scattering of Electromagnetic Waves, Numerical Simulation*. Wiley Series in Remote Sensing. J.A. Kong, Series Editor, 2001.

[2] T.E. Doyle, A.T. Tew, K.H. Warnick, and B.L. Carruth. Simulation of elastic wave scattering in cells and tissues at the microscopic level. *Journal of the Acoustical Society of America*, 125(3):1751–1767, MAR 2009.

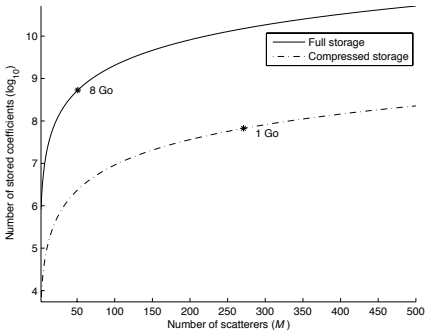

(a) Storage vs. M

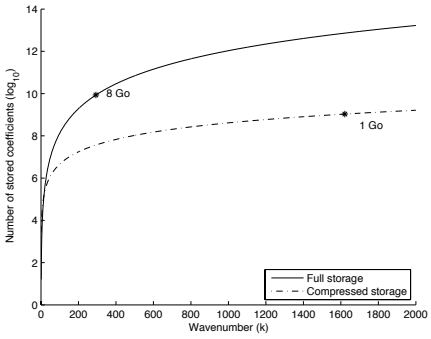

(b) Storage vs. k

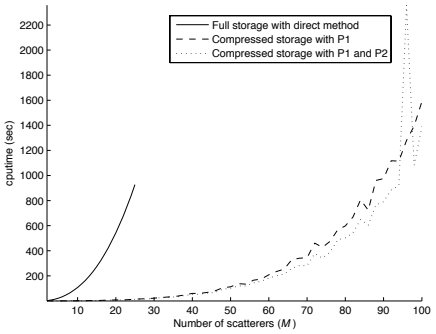

(c) CPU time vs. M

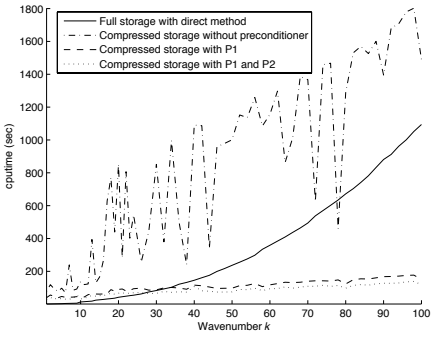

(d) CPU time vs. k

Figure 2: Numerical solution for high-frequencies

[3] R.D. Meade J.D. Joannopoulos and Joshua N. Winn. *Photonic Crystals: Molding the Flow of Light*. 1995.

[4] Y. J. Zhang and E. P. Li. Fast multipole accelerated scattering matrix method for multiple scattering of a large number of cylinders. *Progress in electromagnetics research-PIER*, 72:105–126, 2007.

[5] A. Devilez, B. Stout, N. Bonod, and E. Popov. Spectral analysis of three-dimensional photonic jets. *Optics Express*, 16(18):14200–14212, SEP 1 2008.

[6] P. Ferrand, J. Wenger, A. Devilez, M. Pianta, B. Stout, N. Bonod, E. Popov, and H. Rigneault. Direct imaging of photonic nanojets. *Optics Express*, 16(10):6930–6940, MAY 12 2008.

[7] A. Devilez, N. Bonod, J. Wenger, D. Gerard, B. Stout, H. Rigneault, and E. Popov. Three-dimensional subwavelength confinement of light with dielectric microspheres. *Optics Express*, 17(4):2089–2094, FEB 16 2009.

[8] P. Hewageegana and V. Apalkov. Second harmonic generation in disordered media: Random resonators. *Physical Review B*, 77(7), FEB 2008.

[9] S. Bidault, F.J.G. de Abajo, and A. Polman. Plasmon-based nanolenses assembled on a well-defined DNA template. *Journal of the American Chemical Society*, 130(9):2750+, MAR 5 2008.

[10] H. Mertens, A. F. Koenderink, and A. Polman. Plasmon-enhanced luminescence near noble-metal nanospheres: Comparison of exact theory and an improved Gersten and Nitzan model. *Physical Review B*, 76(11), SEP 2007.

[11] T.E. Doyle, D.A. Robinson, S.B. Jones, K.H. Warnick, and B.L. Carruth. Modeling the permittivity of two-phase media containing monodisperse spheres: Effects of microstructure and multiple scattering. *Physical Review B*, 76(5), AUG 2007.

[12] P. A. Martin. *Multiple scattering*, volume 107 of *Encyclopedia of Mathematics and its Applications*. Cambridge University Press, Cambridge, 2006. Interaction of time-harmonic waves with N obstacles.

[13] X. Antoine, C. Geuzaine, and K. Ramdani. *Wave Propagation in Periodic Media. Analysis, Numerical Techniques and Practical Applications*, volume 1 of *Progress in Computational Physics, pp.73-108*, chapter Computational methods for multiple scattering at high frequency with applications to periodic structure calculations. Bentham Science Publishers Ltd., 2010. (eISBN: 978-1-60805-150-2, 2010).

[14] C Geuzaine, O Bruno, and F Reitich. On the $\mathcal{O}(1)$ solution of multiple-scattering problems. *IEEE Trans. Magn.*, 41(5):1488–1491, MAY 2005. 11th IEEE Biennial Conference on Electromagnetic Field Computation, Seoul, South Korea, Jun 06-09, 2004.

[15] X. Antoine, C. Chniti, and K. Ramdani. On the numerical approximation of high-frequency acoustic multiple scattering problems by circular cylinders. *J. Comp. Phy.*, 227:1754–1771, 2008.

[16] D. L. Colton and R. Kress. *Inverse acoustic and electromagnetic scattering theory*, volume 93 of *Applied Mathematical Sciences*. Springer-Verlag, Berlin, second edition, 1998.

[17] W. McLean. *Strongly elliptic systems and boundary integral equations*. Cambridge University Press, Cambridge, 2000.

[18] R. Kress. Minimizing the condition number of boundary integral operators in acoustic and electromagnetic scattering. *Quart. J. Mech. Appl. Math.*, 38(2):323–341, 1985.

[19] B. Thierry. Ph.D. Thesis. Nancy-Université, France, 2010. Ongoing.

[20] M. Abramowitz and I.A. Stegun. *Handbook of mathematical functions with formulas, graphs, and mathematical tables*, volume 55 of *National Bureau of Standards Applied Mathematics Series*. For sale by the Superintendent of Documents, U.S. Government Printing Office, Washington, D.C., 1964.

[21] Y. Saad and M.H. Schultz. GMRES: a generalized minimal residual algorithm for solving nonsymmetric linear systems. *SIAM J. Sci. Statist. Comput.*, 7(3):856–869, 1986.